# Appendix A

# Electromagnet analysis

## A.1 Electromagnet steady-state flux circuit analysis

In order to determine the static lift force characteristic of the electromagnet, it is necessary to determine the relationship between applied coil mmf and the resultant mmf across each suspension air gap. This can be achieved by analysing a model of the electromagnet flux circuit. Figure A.1 shows a model of the electromagnet flux circuit which incorporates three flux quantities, namely air gap flux, leakage flux and electromagnet core flux.

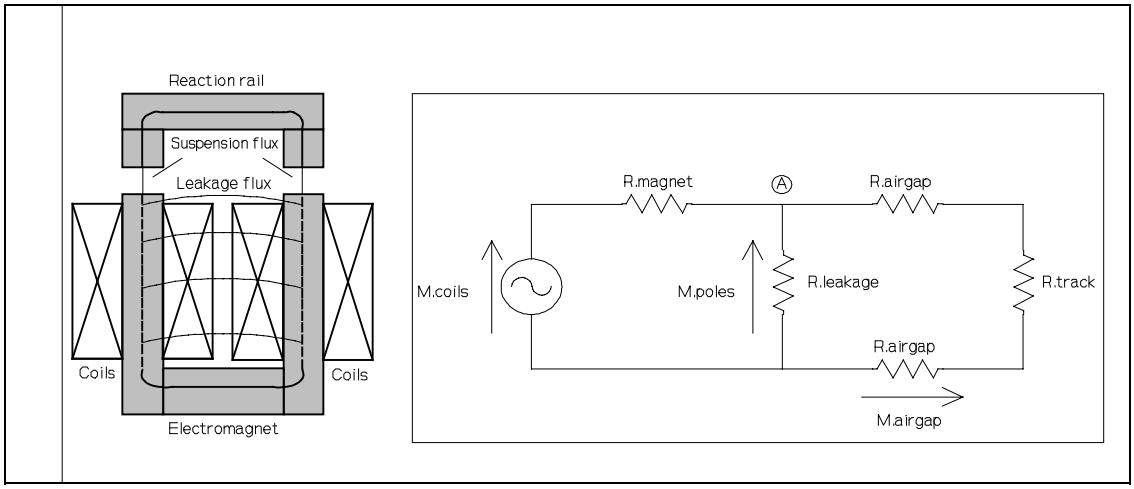


**Figure A.1** Electromagnet flux paths and flux model circuit diagram

Network analysis and the application of Kirchhoff's Current Law is now used to determine the relationship between the applied coil mmf, $M_{coils}$, and the resulting air gap mmf, $M_{airgap}$. First, the currents into node A (see Figure 1) must be summed to zero, giving:

$$\frac{\left(M_{coils} - M_{poles}\right)}{R_{magnet}} + \frac{\left(0 - M_{poles}\right)}{R_{leakage}} + \frac{\left(0 - M_{poles}\right)}{\left(R_{track} + 2R_{airgap}\right)} = 0 \qquad \textbf{A.1}$$

This can be simplified by multiplying by the electromagnet and leakage reluctances,

$$\left(M_{coils} - M_{poles}\right)R_{leakage} - M_{poles}R_{magnet} - \frac{M_{poles}R_{magnet}R_{leakage}}{\left(R_{track} + 2R_{airgap}\right)} = 0 \qquad \textbf{A.2}$$

and collecting terms and rearranging thus,

$$M_{coils}R_{leakage} = M_{poles}\left(R_{leakage} + R_{magnet} + \frac{R_{magnet}R_{leakage}}{\left(R_{track} + 2R_{airgap}\right)}\right) \qquad \textbf{A.3}$$

The mmf across each gap is given by the simple potential divider,

$$M_{airgap} = M_{poles}\left(\frac{R_{airgap}}{R_{track} + 2R_{airgap}}\right) \qquad \textbf{A.4}$$

and hence the pole piece mmf, in terms of the air gap mmf is given by:

$$M_{poles} = M_{airgap}\left(\frac{R_{track} + 2R_{airgap}}{R_{airgap}}\right) \qquad \textbf{A.5}$$

The expression for $M_{poles}$ can now be substituted into Equation 3, giving:

$$M_{coils}R_{leakage} = M_{airgap}\left(\frac{R_{track} + 2R_{airgap}}{R_{airgap}}\right)\left(R_{leakage} + R_{magnet} + \frac{R_{magnet}R_{leakage}}{\left(R_{track} + 2R_{airgap}\right)}\right) \qquad \textbf{A.6}$$

This can be rearranged to give the required relationship between coil mmf and airgap mmf,

$$\frac{M_{airgap}}{M_{coils}} = \frac{R_{leakage}R_{airgap}}{\left(R_{track} + 2R_{airgap}\right)\left(R_{leakage} + R_{magnet}\right) + R_{magnet}R_{leakage}} \qquad \textbf{A.7}$$

## A.2 Eddy current time constant analysis

The flux lag time constant due to eddy-currents circulating within the electromagnet and track cores must be determined before control system synthesis can be performed. A novel time domain analysis is proposed which considers elemental circuits within the core as depicted in Figure A.2. To simplify the analysis, the ferromagnetic core is assumed to have infinite permeability. The analysis is performed in 5 stages, involving the calculation of the following:

- inductance of the elemental circuit within the core.
- inductance of an external coil (ie. outside the core) with a flux coupling equivalent to the internal elemental circuit.
- resistance of the elemental coil.
- time constant of the equivalent external coil circuit.
- total flux lag time constant is obtained by integrating the elemental time constants.

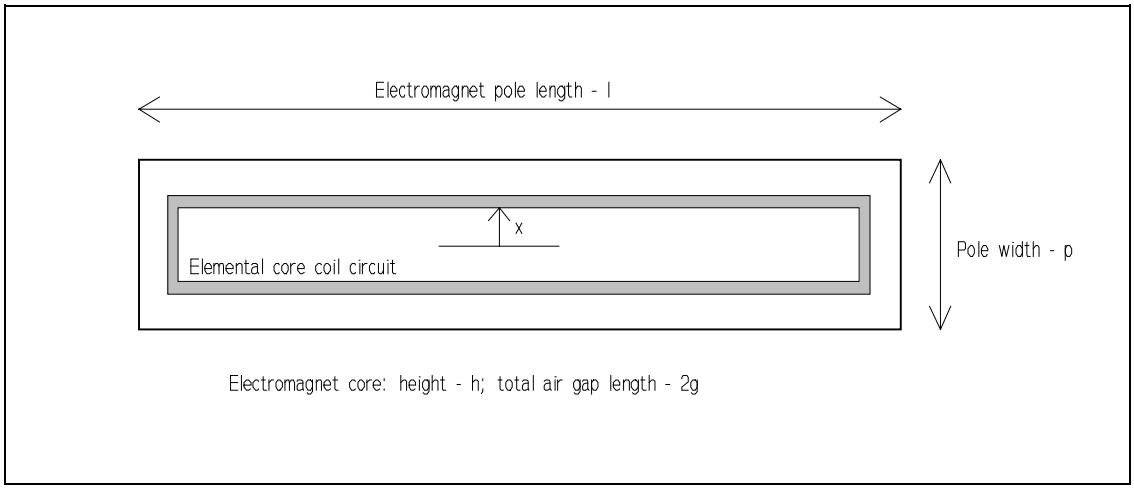


**Figure A.2** Eddy current elemental coil circuit analysis

By assuming infinite core permeability, the self inductance of a cored coil of cross sectional area $A$, with $N$ turns, and a core air gap $g$, is given by:

$$L_{coil} = \frac{\mu_o A N^2}{g} \qquad \textbf{A.8}$$

where $\mu_o$ is the permeability of free space.

The self inductance of the elemental coil circuit within the electromagnet core (with two air gaps) as depicted in Figure A.2 can therefore be approximated by:

$$L_{elem} = \frac{\mu_o 2x\,(l - p + 2x)}{2g} \approx \frac{\mu_o x\, l}{g} \qquad for\ l \gg p,x \qquad \textbf{A.9}$$

The elemental coil inductance must now be translated to the inductance of an external coil coupled to the entire core flux, this is given by:

$$L'_{elem} = L_{elem}\left(\frac{2x}{p}\right) = \frac{2\mu_o x^2 l}{pg} \qquad \textbf{A.10}$$

The resistance of the elemental coil circuit is given by:

$$R_{elem} = \frac{\rho\,(2l - 2p + 8x)}{h\delta x} \approx \frac{2\rho l}{h\delta x} \qquad for\ l \gg p,x \qquad \textbf{A.11}$$

where $\rho$ is the resistivity of the core material, and $\delta x$ is the width of the elemental coil.

The time constant for the equivalent external coil circuit is thus given by,

$$T'_{elem} = \frac{L'_{elem}}{R_{elem}} = \frac{2\mu_o x^2 l h \delta x}{2\rho l p g} = \frac{\mu_o h x^2 \delta x}{\rho p g} \qquad \textbf{A.12}$$

Since the equivalent external coil circuit is effectively coupled to the full core flux, the total time flux lag time constant due to eddy currents for all elemental coils is given by summing the time constant for each coil (see next section),

$$T_{eddy} = \sum T'_{elem} = \sum_x \frac{\mu_o h x^2 \delta x}{\rho p g} \qquad \textbf{A.13}$$

This summation can be most accurately and conveniently achieved by integrating the time constant of elemental eddy current coil circuits, giving,

$$T_{eddy} = \int_0^{p/2} \frac{\mu_o h x^2}{\rho p g}\, dx = \frac{\mu_o h}{\rho p g}\left[\frac{x^3}{3}\right]_0^{p/2} = \frac{\mu_o h p^2}{24\rho g} \qquad \textbf{A.14}$$

## A.3 Summation of coil and eddy current time constants

The eddy current circuits analysed in the previous section give rise to a flux lag characteristic which augments the flux lag due to the electromagnet coil circuit.

The eddy current effect has been modelled using equivalent external coils. The electromagnet, therefore, can be modelled as a transformer with two windings consisting of the excitation coil turns and equivalent eddy current circuit turns. By neglecting any leakage inductance, the two windings can be assumed to be perfectly coupled and hence modelled by the first circuit shown in Figure A.3. The second circuit in Figure A.3 has a secondary winding circuit which has been referred with respect to the primary and is therefore equivalent to the first circuit. The second circuit is now used to analyse the combined behaviour of the coil and eddy current circuits.

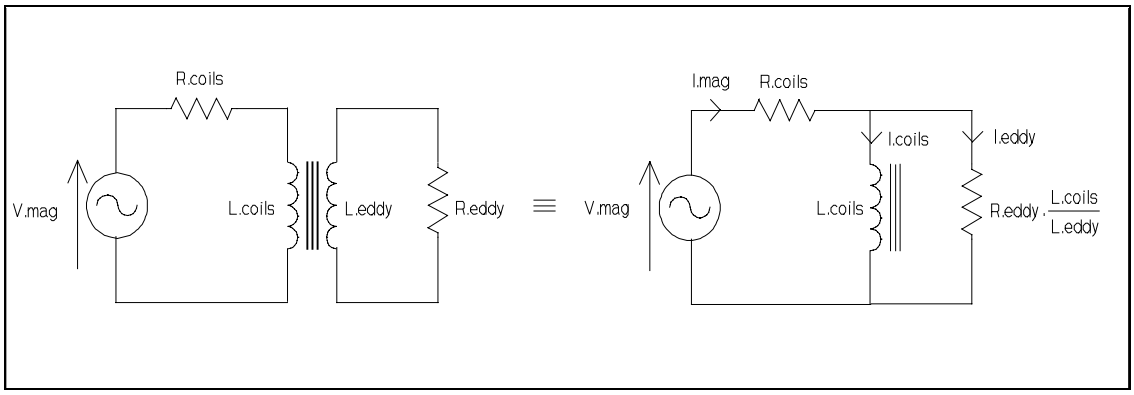


**Figure A.3** Schematic models for the coil and eddy current circuits

For convenience the referred eddy current circuit resistance can be expressed more simply by:

$$R'_{eddy} = \frac{L_{coils}}{T_{eddy}} \qquad where \quad T_{eddy} = \frac{L_{eddy}}{R_{eddy}} \qquad \textbf{A.15}$$

The parallel impedance of the coil inductance and the normalised eddy current circuit resistance is then given by:

$$Z(L_{coils}) \parallel Z(R'_{eddy}) = \frac{sL_{coils}\dfrac{L_{coils}}{T_{eddy}}}{sL_{coils} + \dfrac{L_{coils}}{T_{eddy}}} = \frac{sL_{coils}}{(1+sT_{eddy})} \qquad \textbf{A.16}$$

where *Z(x)* represents the impedance of *x*, and *s* is the Laplace operator.

The voltage across the coil inductance is given by the potential divider:

$$\frac{V_{coils}}{V_{mag}} = \frac{\dfrac{sL_{coils}}{(1 + sT_{eddy})}}{R_{coils} + \dfrac{sL_{coils}}{(1 + sT_{eddy})}} = \frac{s\dfrac{L_{coils}}{R_{coils}}}{\left(1 + sT_{eddy} + s\dfrac{L_{coils}}{R_{coils}}\right)} \qquad \textbf{A.17}$$

Finally, this can be rearranged to express the coil current, $I_{coils}$, in terms of the applied electromagnet voltage, this gives:

$$I_{coils} = \frac{V_{coils}}{sL_{coils}} = \frac{1}{1 + s(T_{coils}+T_{eddy})}\frac{V_{mag}}{R_{coils}} \qquad where \quad T_{coils} = \frac{L_{coils}}{R_{coils}} \qquad \textbf{A.18}$$

The overall flux actuation characteristic is therefore a first-order lag with a time constant equal to the sum of the coil and eddy current time constants.

This result can be expanded in an iterative fashion to prove that any number of perfectly coupled shorted windings will give rise to a first-order flux lag with a time constant equal to the sum of the winding time constants. This fact is used in the previous section to combine the effect of elemental eddy current circuits.

Finally, the transfer function for the referred eddy current, and the total electromagnet current, in terms of the applied electromagnet voltage, are given by the following:

$$I_{eddy} = \frac{V_{coils}}{L_{coils}/T_{eddy}} = \frac{sT_{eddy}}{1 + s(T_{coils}+T_{eddy})}\frac{V_{mag}}{R_{coils}} \qquad \textbf{A.19}$$

$$I_{mag} = I_{coils} + I_{eddy} = \frac{1 + sT_{eddy}}{1 + s(T_{coils}+T_{eddy})}\frac{V_{mag}}{R_{coils}} \qquad \textbf{A.20}$$

## A.4 Computer program to calculate electromagnet model parameter values

```
Program Magnet_Model();

{ Calculates parameter values and forces for the electromagnet model developed in Chapter 2}
{ Pascal Program;  Author: N. S. McLagan; 1-9-90; all variables in elementary units }


{ Electromagnet dimensions }
Const
  length = 0.200;
  pole   = 0.0095;
  offset = 0.0015;
  height = 0.063;
  width  = 0.033;
  num_turns = 274;

  mu_o = 1.2566e-6; { 4e-7.pi }


Function Gap_area( z : Real ) : Real;
  Begin    {Air gap normal plus fringe flux area - from Equation 2.11}
  Gap_area := length * (pole + (2*z / pi))
  End;


Function Lift_force_ratio( z : Real ) : Real;
  Begin    {Electromagnet lift/gross force ratio - Equation 2.20}
  Lift_force_ratio := 1 - (offset/z)*arctan(offset/z) / (1+(pi*pole)/(2*z))
  End;


Function R_mag( mu_m : real ) : Real;
  Begin    {Electromagnet core reluctance - Equation 2.13}
  R_mag := (2*height + width + 2*pole) / (mu_m * mu_o * length * pole)
  End;


Function Mu_mag( core_flux, mu_max, mu_break, mu_span : real ) : Real;

  { mu_max:    Plateau value for mu before roll-off. /1 }
  { mu_break:  Flux density break point for mu roll-off. /Tesla }
  { mu_span:   Span of fall from break point to zero. /Tesla }

  Var
    core_flux_density, mu : Real;
  Begin    {Electromagnet core permeability - Table 2.2}
  mu := mu_max;
  core_flux_density := core_flux / (pole * length);
  IF (core_flux_density > mu_break) Then
    mu := mu * (1 - (core_flux_density - mu_break)/mu_span);
  If (mu < 1) Then
    mu := 1;
  Mu_mag := mu
  End;  { of Mu_mag }


Function R_track( mu_t : Real ) : Real;
  Begin    {Track reluctance - Equation 2.12}
  R_track := (width + 4*pole) / (mu_t * mu_o * length * pole )
  End;


Function Mu_track : Real;
  Begin    {Relative track permeability}
  Mu_track := 2000;
  End;


Function R_leak : Real;
  Begin    {Leakage reluctance - Equation 2.15}
  R_leak := 2*width /( mu_o * (length + 2*width/pi) * (height + 2*width/pi) )
  End;
```

```
Function R_gap( z : real ) : Real;
  Begin    {Air gap reluctance - from Equation 2.11}
  R_gap := z / ( mu_o * Gap_area(z) )
  End;


Function L_mag( z, mu_m, mu_t : Real ) : Real;
  Begin    {Electromagnet inductance - Equation 2.32}
  L_mag := num_turns * num_turns * (R_track(mu_t) + 2*R_gap(z) + R_leak) /
       ((R_track(mu_t)+2*R_gap(z))*(R_leak+R_mag(mu_m))+(R_mag(mu_m)*R_leak))
  End;


Procedure Calculate( Var current, airgap_flux, leakage_flux, core_flux : Real;
               { Using } airgap, force, mu, mu_break, mu_span : Real );
  Var
    gross_force_per_pole : Real;
    pole_mmf, iron_mmf, coil_mmf : Real;

  Begin
  gross_force_per_pole := force / (2 * Lift_force_ratio(airgap));
  airgap_flux  := SQRT( 2*gross_force_per_pole * Gap_area(airgap) * mu_o );
  pole_mmf := airgap_flux * (2 * R_gap(airgap) + R_track( Mu_track ) );
  leakage_flux := pole_mmf / R_leak;
  core_flux  := airgap_flux + leakage_flux;
  iron_mmf := core_flux * R_mag( Mu_mag( core_flux, mu, mu_break, mu_span ) );
  coil_mmf := pole_mmf + iron_mmf;
  current := coil_mmf / num_turns;
  End;  { of Calculate }


Procedure Force;

  Var
    airgap_index : Integer;
    force, airgap : Real;
    airgap_flux, leakage_flux, core_flux : Real;
    current, k : Real;

  Begin
    writeln;
    write( 'Enter required lift force in Newtons: ');
    readln( force );
    writeln;
    For airgap_index := 1 To 9 Do
      Begin
      airgap := airgap_index / 1000;
      Calculate( current, airgap_flux, leakage_flux, core_flux,
                 { Using } airgap, force, 2000, 1.0, 0.6 );
      k := force * airgap * airgap * 1E6 / (current * current);
      write( 'Airgap =', airgap_index:2 );
      write( '  I =',current:7:2 );
      write( '  k =', k:6:2 );
      write( '  track B =', airgap_flux/pole/length:5:2 );
      write( '  mag B =', core_flux/pole/length:5:2 );
      write( '  mu_m =', Mu_mag( core_flux, 2000, 1.0, 0.6 ):5:0 );
      writeln
      End; { of gap loop }
    End;  { of Force }


Procedure Parameters;
  Var
    airgap_index, mu : Integer;
    gap : Real;

  Begin
  mu := 2000;
  writeln;  writeln('All reluctances are kA/Wb, Inductances are in mH' );
  For airgap_index := 0 To 9 Do
    Begin
    gap := airgap_index / 1000;
    writeln;  write( 'Gap = ', airgap_index );
    write( '  R_mag = ',R_mag(mu)/1000:1:0 );
    write( '  R_track = ',R_track(mu)/1000:1:0 );
    write( '  R_leak = ', R_leak/1000:1:0 );
    write( '  2*R_gap = ', 2*R_gap(gap)/1000:4:0 );
    write( '  L_mag =', 1000*L_mag(gap,mu,mu):5:1 );
    write( '   A_gap =', Gap_area(gap):3:3 ); }
    End
  End;  { of Parameters }
```

```
Procedure Spreadsheet_plots;
  Var
    datafile : Text;
    airgap_index, force_index : Integer;
    airgap, force : Real;
    current_fo, current_imu, current_fmu, current_vmu : Real;
    airgap_flux, leakage_flux, core_flux : Real;

  Begin
  writeln;
  writeln( 'Writing spreadsheet data to file: magmodel.dat ' );
  write( 'Airgaps: ');
  Assign( datafile, 'magmodel.dat' );
  Rewrite( datafile );
  For airgap_index := 1 To 7 Do
    Begin
    write( airgap_index, ',' );
    For force_index := 0 To 100 Do
      Begin
      airgap := airgap_index / 1000;
      force := force_index * 20;
      current_fo := SQRT(4*force/(mu_o*pole*length))*airgap/num_turns;
      Calculate( current_imu, airgap_flux, leakage_flux, core_flux,
                 { Using } airgap, force, 1E6, 1E6, 1E6 );
      Calculate( current_fmu, airgap_flux, leakage_flux, core_flux,
                 { Using } airgap, force, 2000, 1E6, 1E6 );
      Calculate( current_vmu, airgap_flux, leakage_flux, core_flux,
                 { Using } airgap, force, 2000, 1.0, 0.6 );
      writeln( datafile, force:10:1, current_fo:8:2, current_imu:8:2,
                                     current_fmu:8:2, current_vmu:8:2  );
      End;  { of force loop }
      writeln( datafile )
    End;  { of airgap loop }
    Close( datafile )
  End;  { of Spreadsheet_plots }


Procedure Menu;
  Var
    response : Char;
  Begin
    Repeat
      writeln;
      writeln;
      writeln('Force and flux characteristic');
      writeln('Parameters');
      writeln('Spreadsheet plot file');
      writeln('Quit');
      readln(response);
      Case response Of
        'f','F': Force;
        'p','P': Parameters;
        's','S': Spreadsheet_plots;
        End; { of Case }
    Until (response = 'Q') Or (response = 'q')
  End;  { of Menu }


Begin
Menu
End.
```

## A.5 Electromagnet and rail design parameters

The analysis of the experimental electromagnet described in Chapter 2 provides a good grounding in the fundamental electromagnetic principles and practical issues that are central to the operation of a suspension electromagnet. This section first examines the impact of electromagnet and rail design parameters on the steady-state force and the force dynamics, and then two distinct electromagnet configurations that have evolved are discussed.

### A.5.1 Steady-state force

The air gap flux coupling the electromagnet and its reaction rail generates a force of attraction between the electromagnet and rail. To assist in the understanding of the concepts involved, it is helpful to make two simplifying assumptions. The first assumption is that the electromagnet and rail cores have negligible reluctance relative to the air gaps, and the second is that the air gap flux is uniformly distributed over an area equal to the electromagnet pole face area. Using these approximations, the lift force is proportional to the square power of the air gap flux density multiplied by the total air gap flux area. To get a satisfactory core lift/weight ratio, the core must be operated with a high flux density. Unit magnetic flux density produces a lift force per unit area of about $4\times10^5$ N/m$^2$. This is a 'magnetic pressure' of 4 bar (60 lb/in$^2$) which is comparable with a typical truck tyre pressure. The flux density used and hence the magnetic pressure determines the pole face area required to support a given load. For example, a 1 t lift capacity requires a total electromagnet pole face area of about 250 cm$^2$ at unit flux density.

At the required high operational flux levels, the reluctance of the cores is not negligible relative to the air gap reluctance. Also, for air gap dimensions comparable to the pole width, significant flux fringing occurs giving an effective air gap flux area larger than the pole face area. For accurate modelling, the simplifying assumptions used above are untenable and a more detailed analysis is required.

The coil excitation required to produce unit flux density in the air gap is dominantly determined by the permeability of free space. Thus, approximately 1600 ampere-turns are required per mm of electromagnet air gap (this figure allows for both air gaps). The desired operating air gap range and lift force range thus determine the required coil excitation range. The coil must be able to dissipate the waste heat generated at the

required excitation and also provide an acceptable power/lift ratio so that excessive power controller weight is avoided. Two critical factors are the conductor resistivity and the method of cooling the coils. These factors dictate a nominal operational current density for the windings based on thermal considerations. The coil cross-section and hence the slot area between the pole pieces can be calculated directly from the current density and the ampere-turns. Coils are usually made from copper or aluminium wire or foil. Aluminium is less dense than copper, but it has a higher resistivity, thus requiring a lower current density than copper for a given power dissipation. The lower current density for aluminium is achieved at the expense of a larger coil cross-sectional area which also needs a longer and hence heavier core. A detailed optimisation analysis is therefore required to design for best power/lift and lift/weight ratios.

In addition to the air gap flux linking the electromagnet and rail, flux also flows across the slot between the pole pieces, increasing the flux through the cores. If the slot is too narrow, this leakage flux requires a larger, heavier core, whereas if it is too wide, the extra yoke length also increases the core weight. The amount of leakage flux is also affected by the location of the coils which can be wound either around the pole pieces or around the yoke. With the coils on the pole pieces, the m.m.f. rises up the pole pieces from 0% at the yoke to 100% at the pole faces. However, with a yoke wound coil, the full m.m.f. is present all the way up the pole pieces. The first arrangement benefits from a smaller leakage flux, thus requiring a smaller and lighter core, whilst the latter arrangement allows a modest increase in the pole face length and area without increasing the yoke and coil size and weight. The optimum slot width/height ratio and the coil location clearly depends on the detailed electromagnet configuration and dimensions.

The partitioning of the coil cross-section into a particular number of turns depends largely on a practical consideration of available power semiconductor technology. From a heat transfer viewpoint, a solid coil consisting of one turn would be ideal. However, such a high current and low voltage coil would obviously require rather a heavy and inefficient power controller and interconnecting cables ! To enable the use of light and economical power controllers, the voltage and current rating of the coil must be matched for use with available power semiconductor technology. The slot space occupied by insulation, and the thermal insulation attendant with electrical insulation must be factored into the allowable coil current density discussed above.

The lift force characteristic outlined above assumes the electromagnet and its rail are vertically aligned. If the electromagnet is displaced laterally so that there is some

overlap of the poles, then the shear flux near the pole edges produces a lateral force component in addition to a reduced lift force component. By using an inverted U-shaped rail core, shear flux occurs at both electromagnet pole faces when the electromagnet and rail are laterally displaced. This rail core shape gives approximately double the lateral force, but at the expense of a reduced lift force because of the increased air gap reluctance. For small lateral displacements (relative to the pole width), the lateral force is approximately proportional to the displacement, thus giving a reasonably constant lateral stiffness. The lateral force and hence stiffness do however decrease as the air gap increases. Accurate modelling of the lateral force for a given pole face geometry, lateral displacement and electromagnet air gap requires a detailed analysis of the air gap flux distribution.

Having considered the design parameters which affect the steady-state force characteristics of suspension electromagnets, the parameters affecting the rate of change of flux must now be considered to determine the dynamic force characteristics.

### A.5.2 Force dynamics

Electromagnet flux changes from one steady-state value to a new steady-state value whenever the air gap or the applied coil terminal voltage changes. The variation in the electromagnet core flux generates an e.m.f. across any conducting circuits that enclose the flux. For a suspension electromagnet, there are two such circuits. The first is the excitation coil circuit, whilst the second circuit occurs within the core material in which circulating eddy currents are distributed. The coil inductance and resistance impose a first order lag characteristic on the core flux with the time constant given by the inductance / resistance ratio. The flux lag due to eddy currents in the core can be approximated by integrating the effect of elemental circuits within the core. This produces a first order flux lag with a time constant proportional to the square power of the smallest pole face dimension divided by the resistivity of the core material. The combined effect of the flux coupled circuits is a first order flux lag characteristic, with a time constant equal to the sum of the coil and core lag time constants. Both the coil inductance and the effective eddy current circuit inductance are a function of the magnetic reluctance of the flux path and hence the air gap length. The flux lag time constant is therefore inversely proportional the air gap length.

The dynamic requirements and structure of the closed-loop suspension controller determine acceptable flux lag time constants for the electromagnet coil and core. There

is little design flexibility with the coil time constant since the coil inductance is fundamentally determined by the air gap reluctance and the coil resistance is generally designed on the basis of coil weight and steady-state power dissipation. The number of coil turns offers no help since doubling the number of turns doubles both the inductance and resistance (assuming a constant coil cross section) leaving the time constant unchanged.

The flux lag time constant due to eddy currents in electromagnet/rail cores depends critically on the shape and size of the pole faces. The time constant can be reduced using a suitable feedback strategy, but if necessary, it is usually more cost effective to modify the core. This can be achieved through the use of high silicon steel (which has a larger resistivity than mild steel) or by using a laminated core construction to reduce the dimensions of the eddy current circuits within the core.

Eddy currents also affect the motion of an electromagnet along its rail. This is because eddy currents in the rail cause a lag in the magnetisation and subsequent demagnetisation of the rail as an electromagnet progresses along the guideway. These spatial flux lags reduce the lift force and generate a drag force. The time a moving electromagnet takes to pass a point on its rail is given by the electromagnet length divided by its speed. As this passing time decreases towards the flux lag time constant of the rail core, the problem becomes more severe. This problem thus increases with higher speeds, shorter magnets and longer rail core time constants. It can therefore be alleviated by using longer electromagnets, higher resistivity steel or a laminated track core. Rather than use a very long electromagnet, a series of shorter electromagnets that maintain the rail magnetism over a number of electromagnets often carries practical advantages.

In addition to controlled d.c. excitation of the electromagnet coil, controlled a.c. excitation provides a similar characteristic lift force behaviour. However, by suitably configuring a number of multi-phase a.c. windings, a moving magnetic field can be produced which generates a propulsion force component in addition to the lift force component. Unfortunately, a.c. excitation produces a lower lift force compared with d.c. excitation. This is because the mean amplitude of a sinusoidal flux is $1/\sqrt{2}$ of the d.c. flux level. Since the force is proportional to the square power of the flux, a 50% loss of force results from the use of a.c. rather than d.c. excitation, assuming a given maximum core flux level. A.c. excited cores also suffer from higher leakage flux due to the larger number of narrower slots which are required to accommodate the multi-phase windings. The overall effect is that a.c. excitation requires approximately

double the core size and weight compared with d.c. excitation. The coil must also be larger and heavier since it must encircle the larger core. The rapid cycling of flux associated with typical a.c. excitation means that laminated magnetic steel or iron cores are mandatory. The merits of using an a.c. excited suspension/propulsion electromagnet/motor clearly depend on whether the additional weight and complexity of the combined scheme is less than that required for a separate linear induction/synchronous motor.

The last dynamic effect to be considered is that due to the magnetic hysteresis of the core materials. Hysteresis can be viewed as an effect which modifies the permeability of the core material. It is very difficult to model accurately because it is a nonlinear function of the flux history of the core. Fortunately, the impact of the core hysteresis on the total flux path reluctance can be largely neglected due to the dominance of the air gap reluctance. However, at small air gaps the effect of hysteresis on the lift force is significant and a qualitative consideration must be made when designing the electromagnet suspension control system.

A detailed analysis of an electromagnetic suspension system in terms of the required closed loop bandwidth, vehicle speed and electromagnet deployment is required to determine suitable pole face dimensions, mode of excitation (a.c. or d.c.), and electromagnet and rail core constructions.

### A.5.3 Practical suspension electromagnets

The overview given above of the influence of electromagnet design parameters on both the steady-state and dynamic performance shows the highly interactive nature of suspension electromagnet design. A successful design clearly requires a constrained optimisation, involving all of the critical design factors, and the use of a structured design procedure[1] is a prerequisite. Out of the multitude of possible electromagnet designs, practical and economic considerations have led to the emergence of two distinct configurations. The base configurations both use U-shaped electromagnets with a flat rail to provide a balance between the critical electromagnet parameters listed in Table A.1.

The two configurations which have emerged are characterised by the orientation with which the magnetic flux passes through the rail. This being either perpendicular (transverse flux) or in-line (axial flux) to the rail direction of travel.

**Table A.1** Critical performance parameters for an electromagnetic suspension

| | |
|---|---|
| • Lift force range | • Weight |
| • Operational air gap range | • Power consumption |
| • Lateral force stiffness | • Electromagnet cost |
| • Track velocity range | • Track cost |
| • Flux time constant | |

Achieving an acceptable rail core size for transverse flux electromagnets requires the use of long, narrow electromagnet poles (with a typical pole length/width ratio of about 100). Such pole faces are sufficiently narrow to permit the use of solid steel cores for the electromagnet and rail with an acceptable eddy current flux lag, even at high speeds. The alternative axial flux electromagnet configuration can use a relatively square pole face without incurring a rail size penalty. However, the square pole cross-section causes a large flux lag time constant due to eddy currents circulating within the cores. This necessitates the use of either a high resistivity or laminated core for the axial flux electromagnet and a laminated core for its rail,[2] thus incurring a significant additional cost over a solid steel rail core.

The are two main performance advantages that accrue from the use of relatively square pole faces rather than long, narrow pole faces. Firstly, they have a much smaller perimeter which results in shorter, lighter coils, with the additional benefit of lower power consumption. A shorter pole length also leads to significantly reduced leakage flux between the pole pieces. This enables the electromagnet core size and weight to be reduced. An additional refinement is possible when two or more adjacent axial flux electromagnets are required, since they can be combined to share common inner pole coils. This configuration (referred to as an E-core when two U-cores are combined) reduces the coil weight relative to independent electromagnets.

The axial flux configuration is thus capable of providing a performance improvement over the transverse flux configuration in terms of the electromagnet lift/weight and power/lift ratios. This performance improvement is achieved at the expense of the requirement for a laminated rail core and either a high resistivity or laminated electromagnet core.

In order to provide a feel for practical electromagnet configurations, the parameters of the axial flux electromagnets used on the PMG vehicle[3] at Birmingham, and the transverse flux electromagnets used on the University of Sussex experimental vehicle[4]

are listed in Table A.2. Both vehicles use electromagnets with anodised aluminium foil coils wound around the pole pieces. The superior performance of the axial flux electromagnet is illustrated by its lift/weight ratio which is almost double that of the transverse flux electromagnet.

**Table A.2** Parameters of typical axial flux and transverse flux electromagnets

| Electromagnet Parameters | Axial Flux | Transverse Flux |
|---|---|---|
| **Vehicle** | PMG Birmingham 8t | Sussex University 1t |
| **Lift capacity** | 1 t | ¼ t |
| **Nominal air gap** | 15 mm | 10 mm |
| **Pole face (length × width)** | 100 × 50 mm | 1000 × 12 mm |
| **Number of flux circuits** | 2 | 1 |
| **Slot width** | 100 mm | 100 mm |
| **Electromagnet core** | E-shaped Magnetic steel | U-shaped Mild steel |
| **Rail core** | Laminated Magnetic steel | U-shaped Mild steel |
| **Lift / Weight ratio** | 11 | 6 |
| **Power / Lift ratio** | 3 kW/t | 2.8 kW/t |

The final configuration to be considered is the a.c. excited axial flux electromagnet/motor employed by the combined suspension/propulsion schemes. The induction motor design uses a slotted, laminated electromagnet/motor core excited by multi-phase a.c. windings. The laminated rail incorporates shorted conduction bar coils as found in conventional induction motor rotors. The active track synchronous motor based scheme uses a slotted, laminated rail core, with powered multi-phase a.c. stator coils to provide propulsion and suspension excitation. The matching 'rotor' cores also carry coils which are used to control the suspension lift force. These combined systems have the obvious advantage of not requiring a separate and heavy propulsion motor and aluminium guideway reaction rail. However, a.c. excitation requires double the electromagnet and rail core size and weight plus a much heavier coil compared to d.c. excitation. An additional drawback for the linear induction motor scheme is that the rail cost is higher than a normal laminated rail due to the conduction bars. The extreme expense of the rail core and coils and the associated power controllers for the active

track linear synchronous motor scheme are justified only for very high speed systems. The active track overcomes the problem of trying to supply many megawatts of propulsion power in a non-contacting fashion to a vehicle travelling at speeds of up to 500 km/h. It is interesting to note that the force of attraction between the stator and 'rotor' of the linear synchronous motor would in most other applications probably be regarded as an undesirable parasitic effect.

## A.6 References

1 Sinha, P. K.: 'Electromagnetic suspension: Dynamics & control', Peter Peregrinus, London, Chapter 6, 1987.

2 Yamamura, S. and Yamaguchi, H.: 'Electromagnetic Levitation System by means of salient pole type magnets coupled with laminated slotless rails', *IEEE Trans. on Veh. Tech.*, **VT-39**, 1990, pp 83-7.

3 Nenadovic, V. and Riches, E.E.: 'Maglev at Birmingham Airport: from system concept to successful operation', *GEC Review*, **1**, 1985, pp 3-17.

4 Jayawant, B.V., Sinha, P.K., Wheeler, A.R., Whorlow, R.J. and Willsher, J.: 'Development of a 1-ton magnetically suspended vehicle using controlled d.c. electromagnets', *Proc. IEE, Pt. A*, **123**, 1976, pp 941-8.